Constraining the date of a seasonally ice-free Arctic using a simple model

David Bonan[1,1], Tapio Schneider[1,1], Ian Eisenman[2,2], and Robert C. J. Wills[3,3]

[1]California Institute of Technology
[2]UC San Diego
[3]University of Washington

November 30, 2022

Abstract

State-of-the-art climate models simulate a large spread in the projected decline of Arctic sea-ice area (SIA) over the 21st century. Here we diagnose causes of this intermodel spread using a simple model that approximates future SIA based on present SIA and the sensitivity of SIA to Arctic temperatures. This model accounts for 70-95% of the intermodel variance, with the majority of the spread arising from present-day biases. The remaining spread arises from intermodel differences in Arctic warming, with some contribution from differences in the local sea-ice sensitivity. Using observations to constrain the projections moves the probability of an ice-free Arctic forward by 10-35 years when compared to unconstrained projections. Under a high-emissions scenario, an ice-free Arctic will likely (>66% probability) occur between 2036-2056 in September and 2050-2068 from July-October. Under a medium-emissions scenario, the 'likely' date occurs between 2040-2062 in September and much later in the 21st century from July-October.

Constraining the date of a seasonally ice-free Arctic using a simple model

David B. Bonan[1], Tapio Schneider[1], Ian Eisenman[2], Robert C.J. Wills[3]

[1]Environmental Science and Engineering, California Institute of Technology, Pasadena, California, USA
[2]Scripps Institution of Oceanography, University of California San Diego, La Jolla, California, USA
[3]Department of Atmospheric Sciences, University of Washington, Seattle, Washington, USA

Key Points:

- A model relating future SIA to present SIA and local sea-ice sensitivity is used to explain the intermodel spread in Arctic SIA projections
- Biases in simulating present-day SIA contribute most to the spread, with model differences in Arctic warming contributing the rest
- Under a high-emissions scenario, the Arctic will likely be ice-free in September between 2036–2056 and from July–October between 2050–2068

Corresponding author: David B. Bonan, dbonan@caltech.edu

Abstract

State-of-the-art climate models simulate a large spread in the projected decline of Arctic sea-ice area (SIA) over the 21st century. Here we diagnose causes of this intermodel spread using a simple model that approximates future SIA based on present SIA and the sensitivity of SIA to Arctic temperatures. This model accounts for 70–95% of the intermodel variance, with the majority of the spread arising from present-day biases. The remaining spread arises from intermodel differences in Arctic warming, with some contribution from differences in the local sea-ice sensitivity. Using observations to constrain the projections moves the probability of an ice-free Arctic forward by 10–35 years when compared to unconstrained projections. Under a high-emissions scenario, an ice-free Arctic will likely (>66% probability) occur between 2036–2056 in September and 2050–2068 from July-October. Under a medium-emissions scenario, the 'likely' date occurs between 2040–2062 in September and much later in the 21st century from July–October.

Plain Language Summary

Arctic sea ice coverage has declined substantially over the past few decades and is projected to continue to decline over the next century. These projections, however, are marred by large uncertainties which arise primarily due to differences between climate models. In this study, we use a simple model that emulates the future evolution of Arctic sea ice as simulated by climate models to explain where this uncertainty comes from. We show that biases in simulating present-day Arctic sea ice contribute most of the uncertainty, with climate model differences in the simulated amount of Arctic warming contributing much of the rest. We use observations to constrain our simple model and show that under a high emissions scenario it is likely the Arctic will be free of sea ice in September sometime between 2036–2056 and from July to October sometime between 2050–2068. We also show that the emissions pathway impacts the length of ice free summers in the Arctic, indicating a low-emissions pathway will reduce the likelihood of seeing ice-free Arctic summers.

1 Introduction

The rapid loss of Arctic sea ice over the last several decades has been one of the clearest manifestations of climate change. Since the beginning of the satellite record, Arctic sea ice has thinned substantially across all seasons, and its summertime coverage has declined by approximately 50% (Fetterer et al., 2016; Stroeve & Notz, 2018). Because sea ice plays an important role in shaping local ecosystems (Wyllie-Echeverria & Wooster, 1998; Laidre et al., 2008), the life of indigenous populations (Ford & Smit, 2004), and socioeconomic activities in the Arctic (Melia et al., 2016), there has been a concerted effort to determine when the Arctic will become seasonally ice free.

Estimates suggest that the Arctic will most likely be ice free ($<$ 1 million km^2) in September by the end of the 21st century (Boé et al., 2009; Notz, 2015; Jahn, 2018; Niederdrenk & Notz, 2018; Sigmond et al., 2018). But it could be ice free as early as mid-century (Holland et al., 2006; Liu et al., 2013; Notz, 2015; Jahn, 2018; Notz & SIMIP Community, 2020; Diebold & Rudebusch, 2021) or in the 2030s (Wang & Overland, 2009; Overland & Wang, 2013; Snape & Forster, 2014; Diebold & Rudebusch, 2021). The large uncertainties in projections of Arctic sea-ice area (SIA) and the date of an ice-free Arctic arise primarily because of structural differences between state-of-the-art global climate models (GCMs) and how they respond to external forcing (Stroeve et al., 2012; Massonnet et al., 2012; Notz & SIMIP Community, 2020; Årthun et al., 2021; Bonan et al., 2021). Emergent constraints, which rely on statistical relationships between observable aspects of the current climate system and future climate change across GCMs, have been used to reduce this spread (Boé et al., 2009; Massonnet et al., 2012; Hall et al., 2019; Senftleben et al., 2020). They suggest that the Arctic may experience ice free conditions in September at some point between 2045 and 2060. Yet, the factors underpinning some of the proposed emergent constraints are currently poorly understood (Hall et al., 2019); in particular, there has been no satisfactory accounting of the relative importance of the sea ice response to warming versus biases in simulating present-day sea ice.

One conceptually convenient metric to understand Arctic sea-ice changes is the sea ice sensitivity, defined as a change of SIA per degree of global warming (Winton, 2011) or per change in cumulative carbon-dioxide emissions (Notz & Marotzke, 2012; Notz & Stroeve, 2016). Because Arctic SIA has been found to be approximately linearly related to global-mean surface temperatures in individual GCMs (Gregory et al., 2002; Winton, 2011;

Armour et al., 2011; Mahlstein & Knutti, 2012; Rosenblum & Eisenman, 2017), it implies that long-term variations in simulated global warming should be proportional to long-term variations in simulated sea ice retreat, which is indeed seen in GCMs (Mahlstein & Knutti, 2012; Rosenblum & Eisenman, 2016, 2017; Jahn, 2018). This suggests that Arctic SIA at some point in time $A(t)$ can be approximated by

$$A(t) = \overline{A}_c + \gamma \cdot (T(t) - \overline{T}_c) \tag{1}$$

where $\overline{A}_c$ is the climatological SIA in a specific reference period, γ is the sea ice sensitivity, and $T(t) - \overline{T}_c$ is the amount of warming relative to the climatological temperature $\overline{T}_c$ in the reference period. The sea ice sensitivity γ can be obtained from the observational record via regression analysis (e.g., Niederdrenk & Notz, 2018). GCMs suggest, at least for annual-mean data, that γ is fairly constant in time (Winton, 2011; Mahlstein & Knutti, 2012), implying that the observational record can be used to estimate the true sea ice sensitivity. However, because SIA relates more directly to Arctic warming than to global warming (Olonscheck et al., 2019; Ding et al., 2019), we go a step further and interpret $T(t) - \overline{T}_c$ as Arctic (60°N–90°N) temperature changes instead of as global temperature changes. We therefore interpret γ as the *local* sea ice sensitivity, defined as a change of SIA per degree of Arctic warming. Variations in annual Arctic SIA from 1979–2020 are well approximated by this expression given observed Arctic surface temperature variations and an estimated (total least squares regression) local sea ice sensitivity $\gamma = -0.80 \times 10^6$ km^2 °C^{-1} (Fig. 1a). The expression accounts for not only the long-term trend and year-to-year variations ($r = 0.96$), but also the detrended variability ($r = 0.81$), which is thought to be crucial for determining when the Arctic will be ice free (Jahn et al., 2016; Screen & Deser, 2019). From 1979–2020, Eq. (1) with monthly estimates of γ also accounts for variations in SIA at monthly timescales, capturing the large downward trend of Arctic SIA in the summer, the more muted decline in the winter, and the interannual variations of Arctic SIA across all months (Fig. 1c and 1d). However, on monthly timescales, it is less clear if the observed local sea ice sensitivity remains constant in time (Mahlstein & Knutti, 2012).

That Eq. (1) captures the trend and variability of observed Arctic SIA over the past few decades suggests that it could also be used to explain the behavior of coupled GCMs. According to Eq. (1), the spread among GCMs could arise from differences in the mean-state SIA of each GCM ($\overline{A}_c$), in the sensitivity of sea ice to Arctic temperature changes (γ), or in the amount of Arctic warming $T(t) - \overline{T}_c$. What can we make of the intermodel spread in projections of Arctic SIA, and how does each term contribute to the total uncertainty? If,

for instance, mean-state biases were reduced across GCMs, how much would this reduce the uncertainty in the date of an ice-free Arctic? Indeed, the mean SIA and the sensitivity of sea ice to global temperature changes in each GCM have been shown to be well correlated with the date of an ice-free Arctic (Massonnet et al., 2012; Jahn, 2018; Notz & SIMIP Community, 2020). For example, Notz & Community, (2020) show that considering only GCMs that correctly simulate both the mean September Arctic SIA and observed sensitivity of September Arctic SIA to cumulative CO_2 emissions suggests the Arctic will be ice-free in September before mid-century, regardless of the emissions scenario. However, previous work has shown that GCMs can match observations for the wrong reasons (e.g., Rosenblum & Eisenman, 2017), suggesting that including only GCMs that correctly simulate certain observed criteria may impact estimates of when an ice-free Arctic will occur. Instead of neglecting GCMs that do not meet certain observational criteria, future projections should be constrained in a systematic manner that includes physically justifiable constraints.

To address these questions, we use Eq. (1) to introduce a simple framework for partitioning model uncertainty in 21st century projections of Arctic SIA into contributions from $\overline{A}_c$, γ, and $T(t) - \overline{T}_c$. This work builds on previous work (e.g., Mahlstein & Knutti, 2012; Jahn, 2018; Notz & SIMIP Community, 2020) by constructing a simple model that further exploits the linear relationship between Arctic SIA and Arctic temperatures and shows how observations can be used to systematically reduce uncertainty in model projections of Arctic sea ice. We then use observations to constrain the individual factors of our simple model, which facilitates conclusions regarding the probability of seeing an ice-free Arctic in the coming decades.

2 Methods

2.1 Observations

Monthly Arctic SIA from 1979 to 2020 was derived using observations of monthly sea ice concentration from the National Snow and Ice Data Center passive microwave retrievals bootstrap algorithm (Fetterer et al., 2016). For observation-based data of near-surface air temperature in the Arctic, we use the ERA5 global reanalysis (Hersbach et al., 2020). We use reanalysis data due to sparse data coverage of the Arctic toward the beginning of the satellite era. Monthly Arctic temperatures from 1979 to 2020 are obtained by calculating the average near-surface air temperature from 60°N to 90°N.

2.2 CMIP6 and large ensemble output

We analyze all CMIP6 GCMs (Eyring et al., 2016) that provide monthly output of sea ice concentration ('siconc') and near-surface air temperature ('tas') for Historical, SSP1-2.6, SSP2-4.5, and SSP5-8.5 simulations (29 different GCMs; see Supplementary Table 1). The Historical simulations (1850–2014) are merged with the SSP simulations (2015–2100). For each GCM, we use sea ice concentration to compute monthly Arctic SIA. Arctic temperatures are calculated as the average near-surface air temperature from 60°N to 90°N. We focus on single ensemble members from each GCM to mitigate over-weighting with respect to one GCM.

We use the 50-member Canadian Earth System Model Large Ensemble Version 5 (CanESM5-LE; Swart et al., 2019) to quantify how internal variability impacts estimates of when the Arctic first becomes seasonally ice free. The CanESM5-LE contains 50 ensemble members each for SSP1-2.6, SSP2-4.5, and SSP5-8.5 forcing, enabling us to estimate internal variability ranges unique to each forcing scenario. Internal variability has been shown to increase as forcing decreases (Jahn, 2018). From each member, we use sea ice concentration to compute monthly SIA.

2.3 Components of the simple model

Eq. (1) contains three components that are diagnosed from observations and the CMIP6 GCMs. The average Arctic SIA for a specific reference period $\overline{A}_c$ is calculated as the time-mean Arctic SIA from 1979–2020 for each month in all GCMs and in observations. The local sea ice sensitivity γ is defined as the change of SIA per degree of Arctic (60°N–90°N) warming. This formulation enables us to capture inter-annual variability of SIA related to Arctic temperature variability that is not captured when using the global-mean (Winton, 2011) or Northern Hemisphere mean (Armour et al., 2011). For each month, γ is computed using total least squares regression from 1979–2020 in observations and 1979-2100 in the CMIP6 GCMs for all values of SIA above 1 million km^2, following Winton, (2011). GCMs show more negative values of γ in the future; Figure S1 shows how the local sea ice sensitivity for each GCM evolves in time from 1979 up to the particular date for the months of July, August, September, and October, where γ is computed from 1979 to the date of interest. In order to constrain γ based on observations, we normalize the multi-model mean of these timeseries by dividing by the first value and multiplying by the observed value.

This constrains the GCMs based on the observed sensitivity and guides the equation how γ evolves into the future. Finally, $\overline{T}_c$ is the average Arctic temperature from 1979–2020 in each GCM and in observations, and $T(t)$ is the Arctic temperature for a given year and month.

2.4 Analysis of variance

The ability of Eq. (1) to explain the intermodel spread in CMIP6 Arctic SIA projections is computed as the proportion of the variance (r^2, where r is the Pearson correlation coefficient) in monthly Arctic SIA from CMIP6 GCMs that is explained by Eq. (1) as a function of year and month. To examine the contribution of each term in Eq. (1) to the intermodel spread of Arctic SIA projections, we use the propagation of uncertainty to quantify the effect of uncertainty from each variable on the total uncertainty. Specifically, we apply the full intermodel spread of one term and hold the other two terms at their multi-model mean values yielding three sets of time series for $A(t)$, each containing 29 realizations, which are the result of the intermodel spread of each individual term. Assuming linearity and that the factors are uncorrelated, the total variance for a given month m and year y is

$$T(m, y) = M(m, y) + S(m, y) + W(m, y) \tag{2}$$

where the fractional uncertainty from a given source is calculated as M/T, S/T, and W/T. M is calculated as the variance due to the intermodel spread in $\overline{A}_c$, S is calculated as the variance due to the intermodel spread in γ, and W is calculated as the variance due to the intermodel spread in $T(t) - \overline{T}_c$. The covariance terms are small and vary between 5–31%, which can be confirmed by calculating the residual between Fig. 2a and the variance explained by the sum of the three individual terms.

2.5 Probability density functions

The date of an ice-free Arctic is taken to be the first year when SIA falls below the 1 million km^2 threshold (Wang & Overland, 2009). This threshold, rather than zero, is commonly used since some sea ice may remain along the northern coasts of Greenland and Ellesmere Island after the bulk of the Arctic Ocean becomes open water. The probability P can be obtained as

$$P\left(t\right) = \int_{t_0}^{t} \frac{1}{\sqrt{2\pi\sigma^2}} e^{\frac{-(t-\mu)^2}{2\sigma^2}} dt \tag{3}$$

where μ is the multi-model mean ice-free date of the CMIP6 GCMs, σ is the standard deviation ice-free date of all CMIP6 GCMs, and t_0 is the beginning of each simulation. Because some GCMs do not project ice-free conditions in the 21st century, each probability is normalized by the number of GCMs used relative to the total number of GCMs, which makes this analogous to the cumulative frequencies of GCMs being ice-free. In this paper, we adopt the IPCC likelihood scale where 'very unlikely' means 0–10%, 'unlikely' means 0–33%, 'as likely as not' means 33–66%, 'likely' means 66–100%, and 'very likely' means 90–100%.

3 Sources of uncertainty in model projections of Arctic sea ice

We first apply Eq. (1) to simulations in Phase 6 of the Coupled Model Intercomparison Project (CMIP6) (Eyring et al., 2016) with Historical and SSP5-8.5 forcing (see Section 2 for more details). Over all months, the proportion of variance across the GCMs that Eq. (1) accounts for varies between 70% and 95% during 2020–2100 (Fig. 2a). The period in which Eq. (1) accounts for the lowest fraction of intermodel variance occurs in early summer during the beginning of the 21st century, when approximately 70–80% of the intermodel variance is captured. Eq. (1) accounts for the most (>90%) intermodel variance in late fall and early winter, likely because model-to-model variations in climatological Arctic SIA are largest in the wintertime (Davy & Outten, 2020; Shu et al., 2020). Arctic SIA calculated from Eq. (1) also bears a striking similarity to the trajectory of each individual GCM for the summer months (Supplemental Figure S2), which is the primary season of interest in this study.

The ability of Eq. (1) to capture most of the intermodel variance suggests the three terms in Eq. (1) can be used to identify sources of intermodel spread in projections of Arctic SIA. Isolating the intermodel spread of each term (see Section 2 for more details) shows that in the near future, biases in present-day SIA ($\overline{A}_c$) account for approximately 70–80% of the total intermodel variance (Fig. 2b). In winter, the effect of mean-state biases persists much longer into the 21st century than in the summer, largely because sea ice remains present, whereas summer sea ice disappears in most GCMs by 2065. In summer, mean-state biases are important initially, accounting for 40–50% of the intermodel spread for the first decade beyond 2020, but their contribution quickly diminishes to approximately 20–30% by 2050. The remaining intermodel spread arises from differences in local sea ice sensitivities (Fig. 2c) and Arctic warming (Fig. 2d). In late fall, model differences in the local sea ice

sensitivity account for approximately 30% of the intermodel variance at the end of the 21st century. Notably, at the summer minimum, the spread in local sea ice sensitivity explains little intermodel variance at the end of the 21st century. The majority of the intermodel spread in September Arctic SIA projections at the end of the 21st century is associated with differences in Arctic warming simulated by GCMs, which accounts for over 80% of the intermodel variance. In winter, variations in Arctic warming begin to matter toward the end of the 21st century and make up approximately 30–40% of the total intermodel variance. Similar results are found for a medium emissions scenario (SSP2-4.5) and a low-emissions scenario (SSP1-2.6), though the relative role of intermodel differences in Arctic warming decreases and accounts for 40–60% of the total summer variance by the end of the 21st century (Supplemental Figure S3–S4).

4 Constraining model projections of Arctic sea ice

We can use Eq. (1) in conjunction with observations to constrain the intermodel spread in projections of Arctic SIA. Satellites have been reliably monitoring Arctic sea ice concentration since 1979, giving estimates of Arctic SIA for more than 40 years. Reanalysis datasets similarly give relatively accurate estimates of Arctic temperatures going back to the early 1950s, when the U.S. Navy and other national meteorological institutes began regular, year-round monitoring of the Arctic. We quantify how these observations constrain projections of an ice-free Arctic (defined as the first year when each GCM crosses the 1 million^2 km^2 SIA threshold) by fitting a Gaussian distribution to the GCM ensemble (see Section 2 for more details). This is analogous to the cumulative frequencies of GCMs being ice-free (Supplemental Figure S5).

4.1 September

We begin by focusing on September Arctic SIA projections in GCMs, based on Eq. (1), without observational constraints. Under a high-emissions scenario (SSP5-8.5), CMIP6 GCM estimates for the terms on the right-hand side of Eq. (1) suggest that it is 'likely' (>66% probability) the Arctic will experience an ice-free September by 2057 and that it is 'very likely' (>90% probability) the Arctic will experience an ice-free September around 2100 (Fig. 3a). Raw GCM output predicts that these ice-free dates will occur 3-5 years earlier than Eq. (1) (Supplemental Figure S5), implying that Eq. (1) provides a relatively accurate estimate of the simulated behavior.

Correcting for mean-state biases in GCMs by using Eq. (1) with the mean-state of September Arctic SIA from 1979–2020 in observations rather than GCMs, brings forward the 'likely' date by 4 years to 2053 and brings forward the 'very likely' by 30 years (Figure 3a). Note, this mean-state adjustment reduces the likelihood of seeing ice-free conditions in the next few decades. Next, using the observed local sea ice sensitivity γ, rather than that from each GCM in addition to the mean-state correction, moves the 'likely' date of an ice-free Arctic forward by three more years to 2050. The 'very likely' date moves forward by an additional 6 years to 2060. This indicates that GCMs tend to underestimate the local sea ice sensitivity in September.

The monthly local sea ice sensitivity is not constant in time in the GCM simulations; they systematically show increasingly negative values in the future. The more negative γ values could arise from the fact that the relationship between sea ice thickness and area is not perfectly linear. At higher thickness regimes, a change in Arctic temperature would result in a smaller area change, whereas at lower thickness regimes, the same change in Arctic temperature would result in a larger area change. Estimating γ from 1979 up until a particular year yields an estimate of how the local sea ice sensitivity evolves in the future according to state-of-the-art GCMs (see Section 2 for more details). With this added guidance, the 'likely' date of seeing an ice-free Arctic in September moves forward by 4 years to 2046. This constraint moves forward the 'very likely' date of ice free conditions in September by 5 years to 2055, which is close to 50 years sooner than the CMIP6 GCMs suggest. Internal variability, which is calculated from a single-model initial condition large ensemble as three standard deviations of the ice-free probability, adds uncertainty to the ice-free date and implies an error range of approximately $\pm$10 years on these estimates (see Section 2 and Table S2). That is, under a high-emissions scenario, our constraint suggests that an ice-free September in the Arctic is 'likely' to occur between 2036–2056 and 'very likely' to occur between 2045–2065.

The same observational constraints can be applied under medium- and low-emissions scenarios. CMIP6 GCMs in conjunction with Eq. (1) suggest the 'likely' date of an ice-free Arctic in September occurs in 2064 and beyond 2100 for medium- and low-emissions scenarios, respectively (Fig. 3b-c). Applying the same observational constraints on $\overline{A}_c$ and γ shifts this date to 2051 and 2091 for medium- and low-emissions scenarios, respectively. In both the medium- and low-emissions scenarios, correcting for mean-state biases pushes back the date of an ice-free Arctic. Constraining the local sea ice sensitivity with observations

moves forward the date of ice-free conditions for the medium-emissions scenario, but it does relatively little to the low-emission scenario. In both scenarios, the future evolution of the local sea ice sensitivity (diagnosed separately for each emissions scenario) moves forward the date of an ice-free Arctic. When compared to the CMIP6 output, the constraints shift the 'as likely as not' (>33% probability) date for the medium-emissions scenario forward by approximately 7 years and the 'likely' date forward by approximately 15 years (Fig. 3b).

4.2 Late summer and early fall

The seasonality of an ice-free Arctic is a feature of Arctic SIA projections that remains important to quantify, as wildlife like polar bears depend on the number of ice-free days (Molnár et al., 2020). Under a high emissions scenario, CMIP6 GCMs suggest that by 2081 the Arctic will 'likely' experience ice free conditions in July (Fig. 4a). Applying the same constraints on $\overline{A}_c$ and γ for July suggests the 'likely' date of an ice-free July is actually 2052, approximately 30 years sooner than GCMs suggest. This is related to the fact that GCMs have large biases in $\overline{A}_c$ and γ in July when compared to observations. Internal variability changes this estimate to between 2045 and 2060. For August, a similar picture emerges. CMIP6 GCMs suggest the Arctic will 'likely' experience ice free conditions in August by 2060, but the constrained estimate is 2050 with a range of 2041 and 2059 due to internal variability (Fig. 4b). The 'very likely' year is around 2060. All of these estimates are 10–30 years sooner than the GCMs suggest and the 'very likely' date moves forward by almost 50 years. October shows a similar picture to the other months. The 'likely' year of the Arctic experiencing ice-free conditions is 2070 (Fig. 4d). Observational constraints of $\overline{A}_c$ and γ moves forward this year to 2059, more than 10 years sooner than GCMs suggest. The 'very likely' date is around 2071, which is approximately 30 years sooner than raw GCM projections.

Under SSP2-4.5 these constraints suggest the 'likely' date when the Arctic will experience an ice-free July occurs around 2062 (Fig. 4a). For SSP1-2.6, by the end of the 21st century it is 'as likely as not' that the Arctic will experience ice-free conditions in July. Furthermore, the probability of seeing ice-free conditions from July to October is greatly increased when compared to the raw output and will 'likely' occur around 2080 for a medium-emissions scenario. For a low-emissions scenario, at the end of the 21st century, the Arctic will 'likely' be ice free in September but not in other months. This suggests that

the emissions scenario matters for the length of the ice-free season, consistent with Jahn, (2018).

5 Discussion

While previous studies have constrained the intermodel spread in Arctic SIA projections (Wang & Overland, 2009; Boé et al., 2009; Massonnet et al., 2012; Notz & SIMIP Community, 2020), most have done so by neglecting GCMs that poorly simulate present-day Arctic sea ice. The fact that GCMs can match observations for the wrong reasons (e.g., Rosenblum & Eisenman, 2017) suggests studies examining future projections should apply physically meaningful and robust constraints, rather than neglecting GCMs that do not meet certain observational criteria. This may explain why our results differ from the conclusions of Notz & SIMIP Community (2020), who find that after applying observational constraints the majority of GCMs become ice-free by mid-century, even under a low-emissions scenario. Here, we find that the majority of GCMs do not become ice-free until approximately 2080 under a low-emissions scenario. These differences likely arise because we retain more intermodel differences in the simulated amount of Arctic warming and use fewer ensemble members of a single GCM.

This work, however, requires a few caveats. There are uncertainties associated with our observational estimates of Arctic warming and Arctic SIA that may change how well GCMs match observations, and change our observational estimates of γ, particularly at monthly timescales (Niederdrenk & Notz, 2018). We also did not explore the role of model inter-dependency (e.g., Sanderson et al., 2015; Knutti et al., 2017) on these conclusions. Investigation of how uncertainty in observations and model inter-dependency influence the results here should be the subject of future work. Finally, we did not examine the causes of Arctic warming in these GCMs. Previous work suggests GCMs have trouble simulating circulation driven sea ice melt (e.g., Topál et al., 2020; Luo et al., 2021), which may have accounted for 20–40% of observed Arctic sea ice loss (Ding et al., 2019). Future work should study the role of model biases in influencing the evolution of the local sea-ice sensitivity.

6 Summary

This study introduces a simple framework to explain and constrain model projections of Arctic SIA over the 21st century. We find that a simple model (Eq. 1), which approximates future SIA based on present SIA and the sensitivity of SIA to Arctic temperatures, is able to

emulate the evolution of Arctic SIA with remarkable skill. This model accounts for 70–95% of the intermodel variance in projections of Arctic SIA. Isolating the contributing factors shows that the majority of the model uncertainty in projections of Arctic SIA arises from biases in simulating present-day Arctic SIA. The remaining model uncertainty arises from differences in the simulated amount of Arctic warming, with some contribution from differences in the local sea ice sensitivity. This suggests that the degree of Arctic amplification and representation of clouds in these GCMs (e.g., Meehl et al., 2020; Zelinka et al., 2020) may be key to understanding the fate of Arctic sea ice.

Using observations to constrain the individual components of Eq. (1) moves forward the date of an ice free Arctic by 10–35 years when compared to unconstrained projections. Under a high-emissions scenario, the probability of seeing ice-free conditions in the Arctic in September around 2035 is 'as likely as not', and the probability of seeing ice-free conditions in the Arctic in September around 2068 is 'virtually certain' (>99% probability), which is much sooner than climate models suggest. The fate of Arctic sea ice throughout the summertime is similar. The probability of seeing ice-free conditions from July to October around 2059 is 'likely', and it is 'very likely' that the Arctic will experience ice-free conditions that persist from July to October around 2070 under a high-emissions scenario. Thus, this work highlights the importance of considering the length of the potential ice-free period when assessing model projections, not just the date of seeing ice-free conditions in September. Importantly, reducing emissions pushes back the expected dates of ice-free conditions. Under a medium-emissions scenario, the Arctic will 'likely' only experience ice-free conditions from July to October after 2080. Under a low-emissions scenario, the Arctic will 'likely' only be ice free in September at the end of the 21st century. Hence, the emissions scenario determines the length of the ice-free season. Overall, our results show how observations can be used in concert with a simple model to constrain the date of seasonally ice-free conditions in the Arctic Ocean.

Acknowledgments

The authors thank Elizabeth Hunke, Caroline Holmes, and François Massonnet for helpful comments on an earlier draft of this work. The authors also thank two anonymous reviewers and the Editor, Gudrun Magnusdottir, for helpful comments. D.B.B. was supported by an American Meteorological Society (AMS) Graduate Fellowship and the National Science Foundation Graduate Research Fellowship Program (NSF Grant DGE-1745301). Part of

this research was supported by Eric and Wendy Schmidt by recommendation of the Schmidt Futures program. I.E. acknowledges support from the National Science Foundation (Grant OPP-1643445). R.C.J.W also acknowledges support from the National Science Foundation (Grant AGS-1929775). The data that support the findings of this study are freely available from the Earth System Grid Federation (ESGF) (https://esgf-node.llnl.gov/search/cmip6/). The data can be found by searching 'siconc' and 'tas' with the Experiment ID: 'historical', 'SSP126', 'SSP245', or 'SSP585'. Code and data for this research is also available at https://doi.org/10.5281/zenodo.5177172.

References

Armour, K., Eisenman, I., Blanchard-Wrigglesworth, E., McCusker, K., & Bitz, C. (2011). The reversibility of sea ice loss in a state-of-the-art climate model. *Geophysical Research Letters*, *38*(16), L16705.

Årthun, M., Onarheim, I. H., Dörr, J., & Eldevik, T. (2021). The seasonal and regional transition to an ice-free Arctic. *Geophysical Research Letters*, *48*(1), e2020GL090825.

Boé, J., Hall, A., & Qu, X. (2009). September sea-ice cover in the Arctic Ocean projected to vanish by 2100. *Nature Geoscience*, *2*(5), 341–343.

Bonan, D. B., Lehner, F., & Holland, M. M. (2021). Partitioning uncertainty in projections of Arctic sea ice. *Environmental Research Letters*, *16*(4), 044002.

Davy, R., & Outten, S. (2020). The Arctic surface climate in CMIP6: status and developments since CMIP5. *Journal of Climate*, *33*(18), 8047–8068.

Diebold, F. X., & Rudebusch, G. D. (2021). Probability assessments of an ice-free Arctic: Comparing statistical and climate model projections. *Journal of Econometrics*.

Ding, Q., Schweiger, A., L'Heureux, M., Steig, E. J., Battisti, D. S., Johnson, N. C., ... others (2019). Fingerprints of internal drivers of Arctic sea ice loss in observations and model simulations. *Nature Geoscience*, *12*(1), 28–33.

Eyring, V., Bony, S., Meehl, G. A., Senior, C. A., Stevens, B., Stouffer, R. J., & Taylor, K. E. (2016). Overview of the Coupled Model Intercomparison Project Phase 6 (CMIP6) experimental design and organization. *Geoscientific Model Development*, *9*(5), 1937–1958.

Fetterer, F., Knowles, K., Meier, W., Savoie, M., & Windnagel, A. (2016). *Sea Ice Index, Version 3. Boulder, Colorado USA. NSIDC: National Snow and Ice Data Center.*

Ford, J. D., & Smit, B. (2004). A framework for assessing the vulnerability of communities

in the Canadian Arctic to risks associated with climate change. *Arctic*, 389–400.

Gregory, J. M., Stott, P., Cresswell, D., Rayner, N., Gordon, C., & Sexton, D. (2002). Recent and future changes in Arctic sea ice simulated by the HadCM3 AOGCM. *Geophysical Research Letters*, *29*(24), 2175.

Hall, A., Cox, P., Huntingford, C., & Klein, S. (2019). Progressing emergent constraints on future climate change. *Nature Climate Change*, *9*(4), 269–278.

Hersbach, H., Bell, B., Berrisford, P., Hirahara, S., Horányi, A., Muñoz-Sabater, J., ... others (2020). The ERA5 global reanalysis. *Quarterly Journal of the Royal Meteorological Society*, *146*(730), 1999–2049.

Holland, M. M., Bitz, C. M., & Tremblay, B. (2006). Future abrupt reductions in the summer Arctic sea ice. *Geophysical Research Letters*, *33*(23), L23503.

Jahn, A. (2018). Reduced probability of ice-free summers for 1.5°C compared to 2°C warming. *Nature Climate Change*, *8*(5), 409–413.

Jahn, A., Kay, J. E., Holland, M. M., & Hall, D. M. (2016). How predictable is the timing of a summer ice-free Arctic? *Geophysical Research Letters*, *43*(17), 9113–9120.

Knutti, R., Sedláček, J., Sanderson, B. M., Lorenz, R., Fischer, E. M., & Eyring, V. (2017). A climate model projection weighting scheme accounting for performance and interdependence. *Geophysical Research Letters*, *44*(4), 1909–1918.

Laidre, K. L., Stirling, I., Lowry, L. F., Wiig, Ø., Heide-Jørgensen, M. P., & Ferguson, S. H. (2008). Quantifying the sensitivity of Arctic marine mammals to climate-induced habitat change. *Ecological Applications*, *18*(sp2), S97–S125.

Liu, J., Song, M., Horton, R. M., & Hu, Y. (2013). Reducing spread in climate model projections of a September ice-free Arctic. *Proceedings of the National Academy of Sciences*, *110*(31), 12571–12576.

Luo, R., Ding, Q., Wu, Z., Baxter, I., Bushuk, M., Huang, Y., & Dong, X. (2021). Summertime atmosphere–sea ice coupling in the Arctic simulated by CMIP5/6 models: Importance of large-scale circulation. *Climate Dynamics*, *56*(5), 1467–1485.

Mahlstein, I., & Knutti, R. (2012). September Arctic sea ice predicted to disappear near 2°C global warming above present. *Journal of Geophysical Research: Atmospheres*, *117*(D6), D06104.

Massonnet, F., Fichefet, T., Goosse, H., Bitz, C. M., Philippon-Berthier, G., Holland, M. M., & Barriat, P.-Y. (2012). Constraining projections of summer Arctic sea ice. *The Cryosphere*, *6*(6), 1383–1394.

Meehl, G. A., Senior, C. A., Eyring, V., Flato, G., Lamarque, J.-F., Stouffer, R. J., ... Schlund, M. (2020). Context for interpreting equilibrium climate sensitivity and transient climate response from the CMIP6 Earth system models. *Science Advances*, *6*(26), eaba1981.

Melia, N., Haines, K., & Hawkins, E. (2016). Sea ice decline and 21st century trans-Arctic shipping routes. *Geophysical Research Letters*, *43*(18), 9720–9728.

Molnár, P. K., Bitz, C. M., Holland, M. M., Kay, J. E., Penk, S. R., & Amstrup, S. C. (2020). Fasting season length sets temporal limits for global polar bear persistence. *Nature Climate Change*, *10*(8), 732–738.

Niederdrenk, A. L., & Notz, D. (2018). Arctic sea ice in a 1.5°C warmer world. *Geophysical Research Letters*, *45*(4), 1963–1971.

Notz, D. (2015). How well must climate models agree with observations? *Philosophical Transactions of the Royal Society A: Mathematical, Physical and Engineering Sciences*, *373*(2052), 20140164.

Notz, D., & Marotzke, J. (2012). Observations reveal external driver for Arctic sea-ice retreat. *Geophysical Research Letters*, *39*(8).

Notz, D., & Stroeve, J. (2016). Observed Arctic sea-ice loss directly follows anthropogenic CO2 emission. *Science*, *354*(6313), 747–750.

Notz & SIMIP Community. (2020). Arctic Sea Ice in CMIP6. *Geophysical Research Letters*, *47*(10), e2019GL086749.

Olonscheck, D., Mauritsen, T., & Notz, D. (2019). Arctic sea-ice variability is primarily driven by atmospheric temperature fluctuations. *Nature Geoscience*, *12*(6), 430–434.

Overland, J. E., & Wang, M. (2013). When will the summer Arctic be nearly sea ice free? *Geophysical Research Letters*, *40*(10), 2097–2101.

Rosenblum, E., & Eisenman, I. (2016). Faster Arctic sea ice retreat in CMIP5 than in CMIP3 due to volcanoes. *Journal of Climate*, *29*(24), 9179–9188.

Rosenblum, E., & Eisenman, I. (2017). Sea ice trends in climate models only accurate in runs with biased global warming. *Journal of Climate*, *30*(16), 6265–6278.

Sanderson, B. M., Knutti, R., & Caldwell, P. (2015). Addressing interdependency in a multimodel ensemble by interpolation of model properties. *Journal of Climate*, *28*(13), 5150–5170.

Screen, J., & Deser, C. (2019). Pacific Ocean variability influences the time of emergence of a seasonally ice-free Arctic Ocean. *Geophysical Research Letters*, *46*(4), 2222–2231.

Senftleben, D., Lauer, A., & Karpechko, A. (2020). Constraining uncertainties in CMIP5 projections of September Arctic sea ice extent with observations. *Journal of Climate*, *33*(4), 1487–1503.

Shu, Q., Wang, Q., Song, Z., Qiao, F., Zhao, J., Chu, M., & Li, X. (2020). Assessment of sea ice extent in CMIP6 with comparison to observations and CMIP5. *Geophysical Research Letters*, *47*(9), e2020GL087965.

Sigmond, M., Fyfe, J. C., & Swart, N. C. (2018). Ice-free Arctic projections under the Paris Agreement. *Nature Climate Change*, *8*(5), 404–408.

Snape, T. J., & Forster, P. M. (2014). Decline of Arctic sea ice: Evaluation and weighting of CMIP5 projections. *Journal of Geophysical Research: Atmospheres*, *119*(2), 546–554.

Stroeve, J., Kattsov, V., Barrett, A., Serreze, M., Pavlova, T., Holland, M., & Meier, W. N. (2012). Trends in Arctic sea ice extent from CMIP5, CMIP3 and observations. *Geophysical Research Letters*, *39*(16), L16502.

Stroeve, J., & Notz, D. (2018). Changing state of Arctic sea ice across all seasons. *Environmental Research Letters*, *13*(10), 103001.

Swart, N. C., Cole, J. N., Kharin, V. V., Lazare, M., Scinocca, J. F., Gillett, N. P., ... others (2019). The Canadian earth system model version 5 (CanESM5. 0.3). *Geoscientific Model Development*, *12*(11), 4823–4873.

Topál, D., Ding, Q., Mitchell, J., Baxter, I., Herein, M., Haszpra, T., ... Li, Q. (2020). An internal atmospheric process determining summertime Arctic sea ice melting in the next three decades: lessons learned from five large ensembles and multiple CMIP5 climate simulations. *Journal of Climate*, *33*(17), 7431–7454.

Wang, M., & Overland, J. E. (2009). A sea ice free summer Arctic within 30 years? *Geophysical research letters*, *36*(7), L07502.

Winton, M. (2011). Do climate models underestimate the sensitivity of Northern Hemisphere sea ice cover? *Journal of Climate*, *24*(15), 3924–3934.

Wyllie-Echeverria, T., & Wooster, W. S. (1998). Year-to-year variations in Bering Sea ice cover and some consequences for fish distributions. *Fisheries Oceanography*, *7*(2), 159–170.

Zelinka, M. D., Myers, T. A., McCoy, D. T., Po-Chedley, S., Caldwell, P. M., Ceppi, P., ... Taylor, K. E. (2020). Causes of higher climate sensitivity in CMIP6 models. *Geophysical Research Letters*, *47*(1), e2019GL085782.

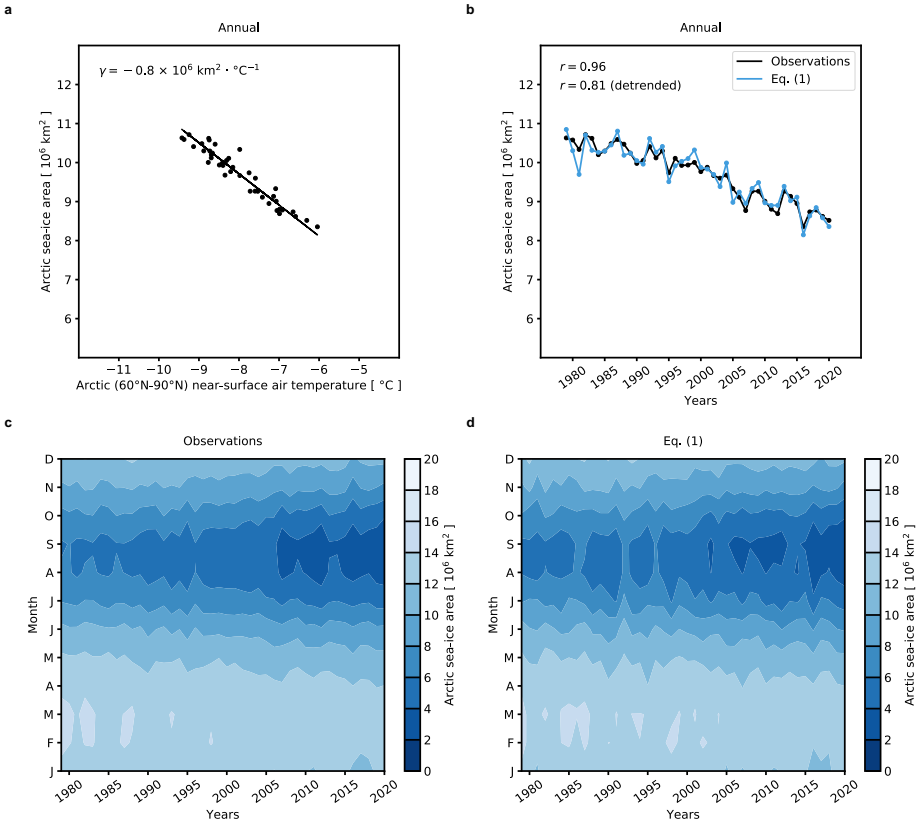

Figure 1. Applying the simple model (Eq. 1) to observations. (a) Scatter plot showing the relationship between observed annual Arctic (60°–90°N) near-surface air temperature and annual Arctic sea-ice area from 1979–2020, implying a local sea ice sensitivity of $\gamma = -0.80 \times 10^6$ km^2 °C^{-1}. (b) Annual Arctic sea-ice area from 1979–2020 in observations (black) and using Eq. (1) with observed temperature variations (blue). The correlation between the two time series is shown in the upper left with and without the linear trend. Monthly Arctic sea-ice area from 1979–2020 in (c) observations and (d) using Eq. (1) with γ estimated for each month.

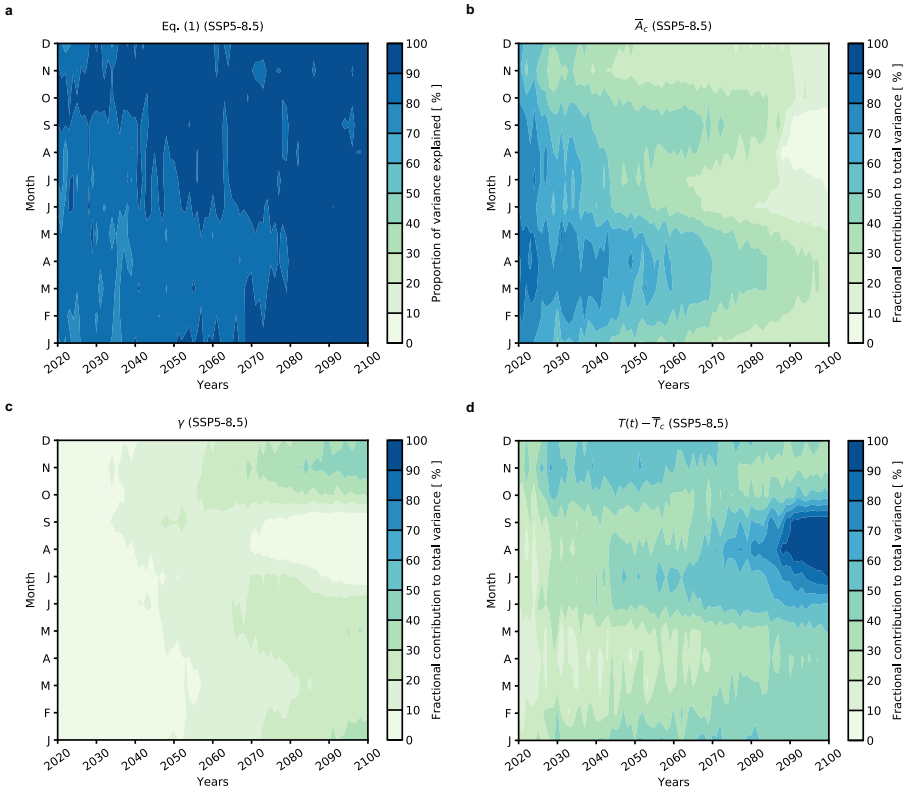

Figure 2. Partitioning intermodel variance in projections of Arctic sea-ice area. (a) The proportion of the intermodel variance (r^2, where r is the Pearson correlation coefficient) in monthly Arctic sea-ice area from CMIP6 SSP5-8.5 simulations that is accounted for by Eq. (1) as a function of month and year. Fractional contribution of (b) $\overline{A}_c$, (c) γ, and (d) $T(t) - \overline{T}_c$ to the total variance for SSP5-8.5 as a function of month and year.

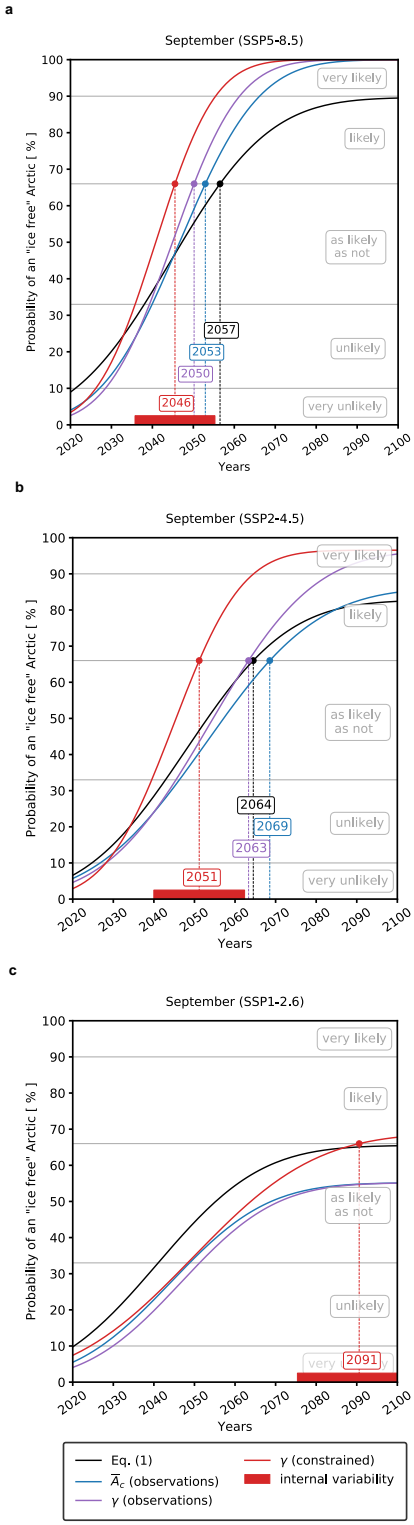

Figure 3. Probability of an ice-free Arctic in September. Cumulative probability density function for the year when the Arctic will experience ice free conditions in September for (a) SSP5-8.5, (b) SSP2-4.5, (c) SSP1-2.6. The black line is the unconstrained Eq. (1) using CMIP6. The blue line is constrained by the mean September Arctic sea-ice area from 1979–2020 in observations. The purple line is constrained by both the mean September Arctic sea-ice area and local sea ice sensitivity from 1979–2020 observations. The red line is the same as the purple line, but with guidance from the GCMs on how the local sea ice sensitivity evolves in the future. The red shading denotes the range due to internal variability estimated from the CanESM5-LE.

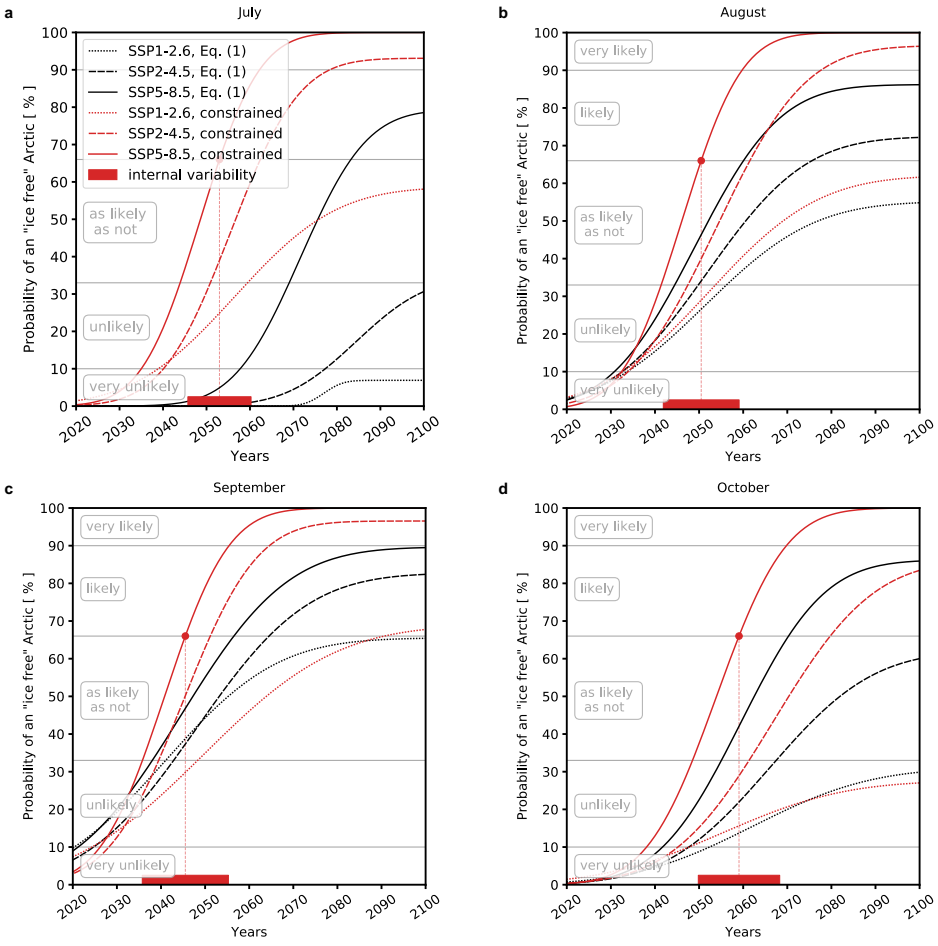

Figure 4. Probability of an ice-free Arctic from July to October. Cumulative probability density function for the year when the Arctic will experience ice free conditions in (a) July, (b) August, (c) September, and (d) October. The black line is the unconstrained Eq. (1) using CMIP6. The red line is the constrained output with the observed $\overline{A}_c$ and γ, and with guidance on how the local sea ice sensitivity evolves in the future (as in Figure 3). The solid lines, dashed lines, and dotted lines denote SSP5-8.5, SSP2-4.5, and SSP1-2.6, respectively. The red shading denotes the range due to internal variability estimated from the CanESM5-LE.

Supporting Information:
Constraining the date of a seasonally ice-free Arctic using a simple model

David B. Bonan[1], Tapio Schneider[1], Ian Eisenman[2], Robert C.J. Wills[3]

[1]Environmental Science and Engineering, California Institute of Technology
[2]Scripps Institution of Oceanography, University of California, San Diego
[3]Department of Atmospheric Sciences, University of Washington

August 10, 2021

Table of Contents

	Model Name	Ensemble Member
1.	ACCESS-CM2	r1i1p1f1
2.	ACCESS-ESM1-5	r1i1p1f1
3.	BCC-CSM2-MR	r1i1p1f1
4.	CAMS-CSM1-0	r1i1p1f1
5.	CanESM5	r1i1p1f1
6.	CESM2	r4i1p1f1
7.	CESM2-WACCM	r1i1p1f1
8.	CNRM-CM6-1-HR	r1i1p1f2
9.	CNRM-CM6-1	r1i1p1f2
10.	EC-Earth3	r1i1p1f1
11.	EC-Earth3-Veg	r1i1p1f1
12.	EC-Earth3-Veg-LR	r1i1p1f1
13.	FGOALS-f3-L	r1i1p1f1
14.	FGOALS-g3	r1i1p1f1
15.	FIO-ESM-2-0	r1i1p1f1
16.	GFDL-ESM4	r1i1p1f1
17.	HadGEM3-GC31-LL	r1i1p1f3
18.	INM-CM4-8	r1i1p1f1
19.	INM-CM5-0	r1i1p1f1
20.	IPSL-CM6A-LR	r1i1p1f1
21.	MIROC6	r1i1p1f1
22.	MIROC-ES2L	r1i1p1f2
23.	MPI-ESM1-2-HR	r1i1p1f1
24.	MPI-ESM1-2-LR	r1i1p1f1
25.	MRI-ESM2-0	r1i1p1f1
26.	NESM3	r1i1p1f1
27.	NorESM2-LM	r1i1p1f1
28.	NorESM2-MM	r1i1p1f1
29.	UKESM1-0-LL	r1i1p1f2

Supplemental Table 1: List of the coupled GCMs and ensemble member used for each Historical, SSP1-2.6, SSP2-4.5, and SSP5-8.5 simulation.

Month	SSP5-8.5	SSP2-4.5	SSP1-2.6
July	15 years	34 years	N/A
August	18 years	21 years	N/A
September	20 years	22 years	30 years
October	18 years	21 years	N/A

Supplemental Table 2: Internal variability range denoting the range of years when ice-free conditions in the Arctic appear as estimated from the 50-member CanESM5 large ensemble. The range denotes the 3-σ spread (0.14% and 99.86%) for each month and each forcing scenario. For SSP1-2.6, July, August, and October are not included as most ensemble members do not experience ice-free conditions.

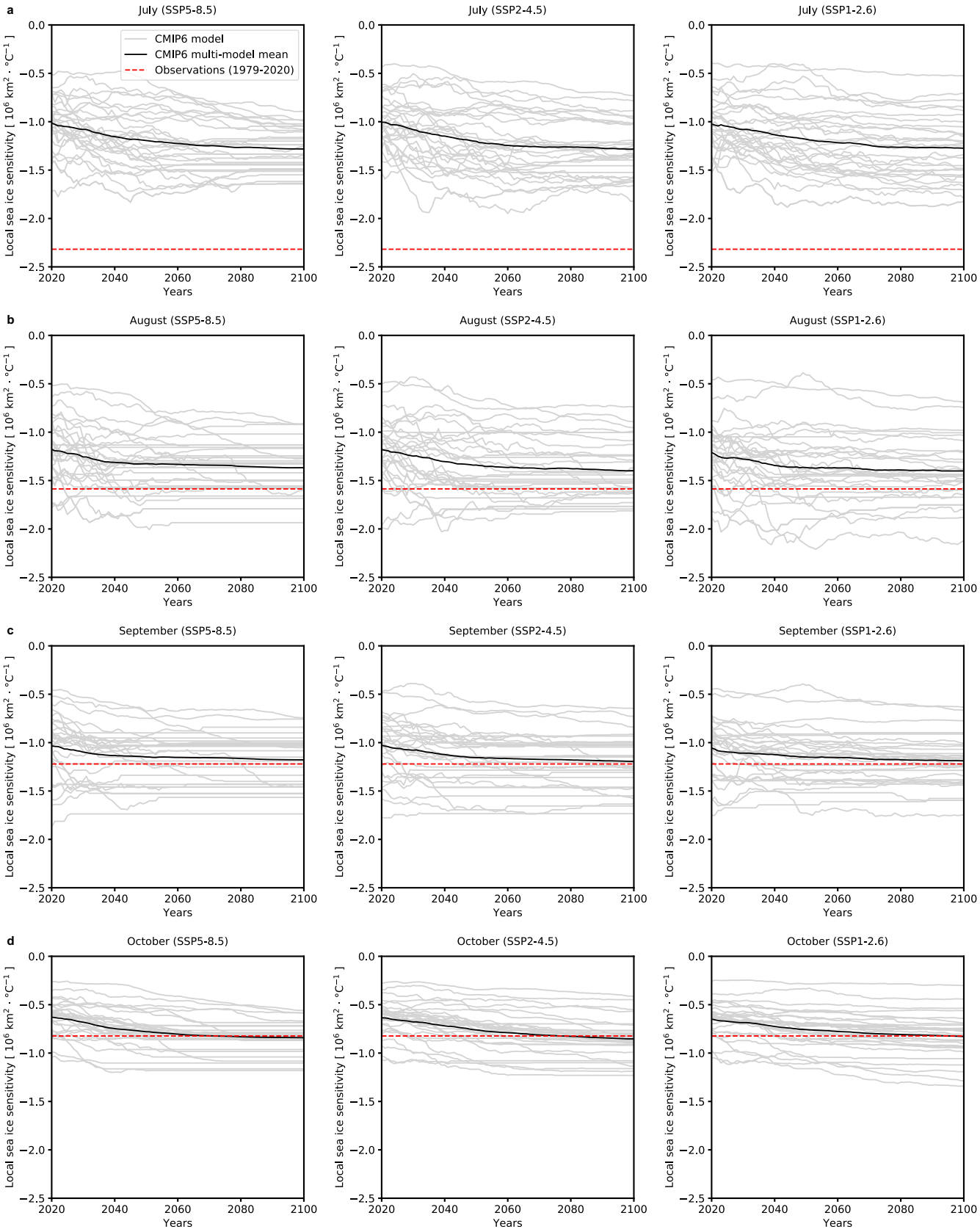

Supplemental Figure 1: **Evolution of the local sea ice sensitivity.** The local sea ice sensitivity for 29 different coupled GCMs computed using total least squares from 1979 up to each year using the month of (a) July, (b) August, (c) September, and (d) October. The black line in each panel denotes the multi-model mean and the grey lines represent individual GCMs. The red dashed line denotes observations from 1979–2020.

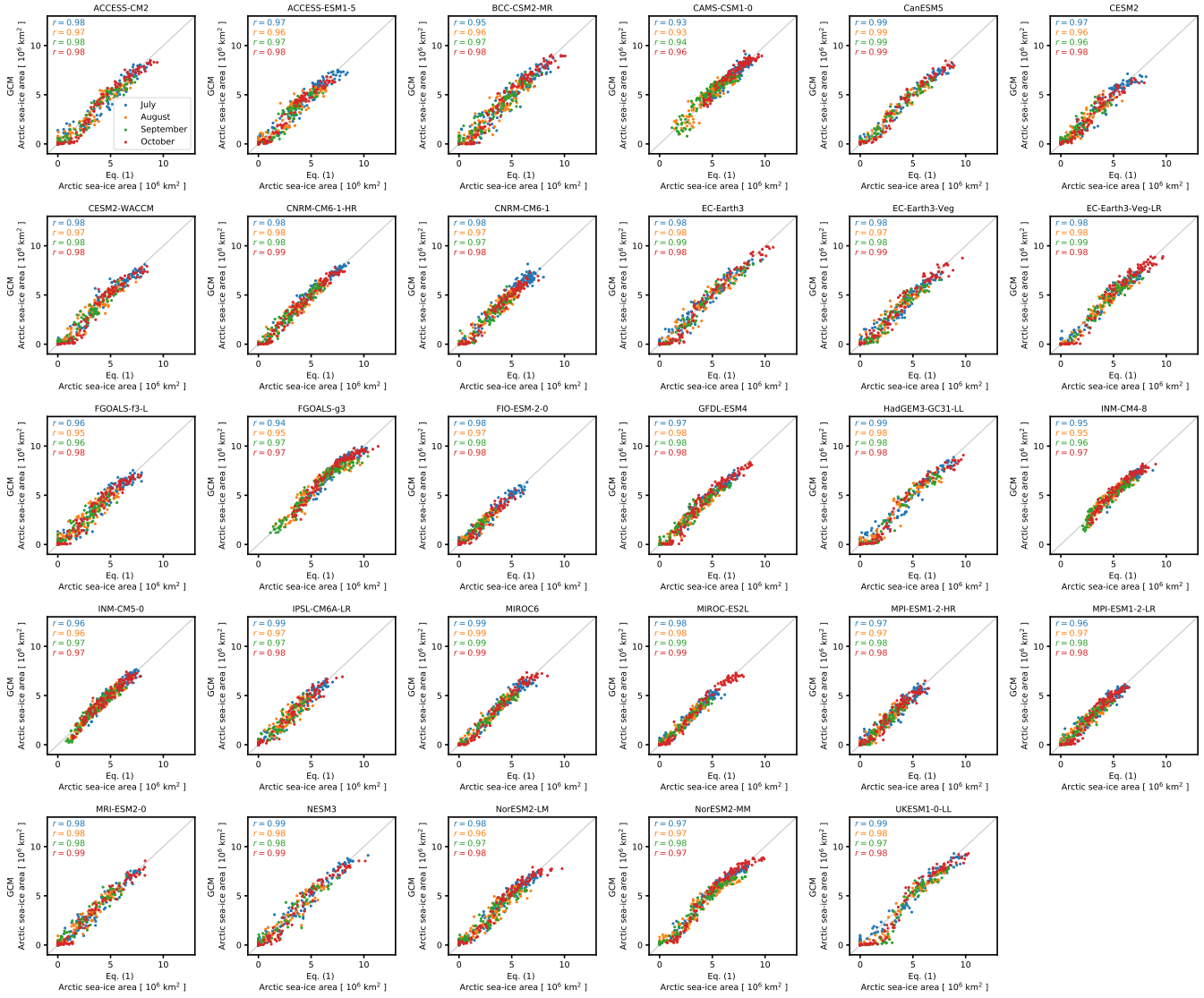

Supplemental Figure 2: **Comparison of Arctic sea-ice area from each GCM and Eq. (1).** Arctic sea-ice area from 29 different coupled GCMs (y-axis) and calculated using Eq. (1) (x-axis) in July (blue), August (orange), September (green), and October (red). All plots use Historical and SSP5-8.5 simulations from 1979–2100.

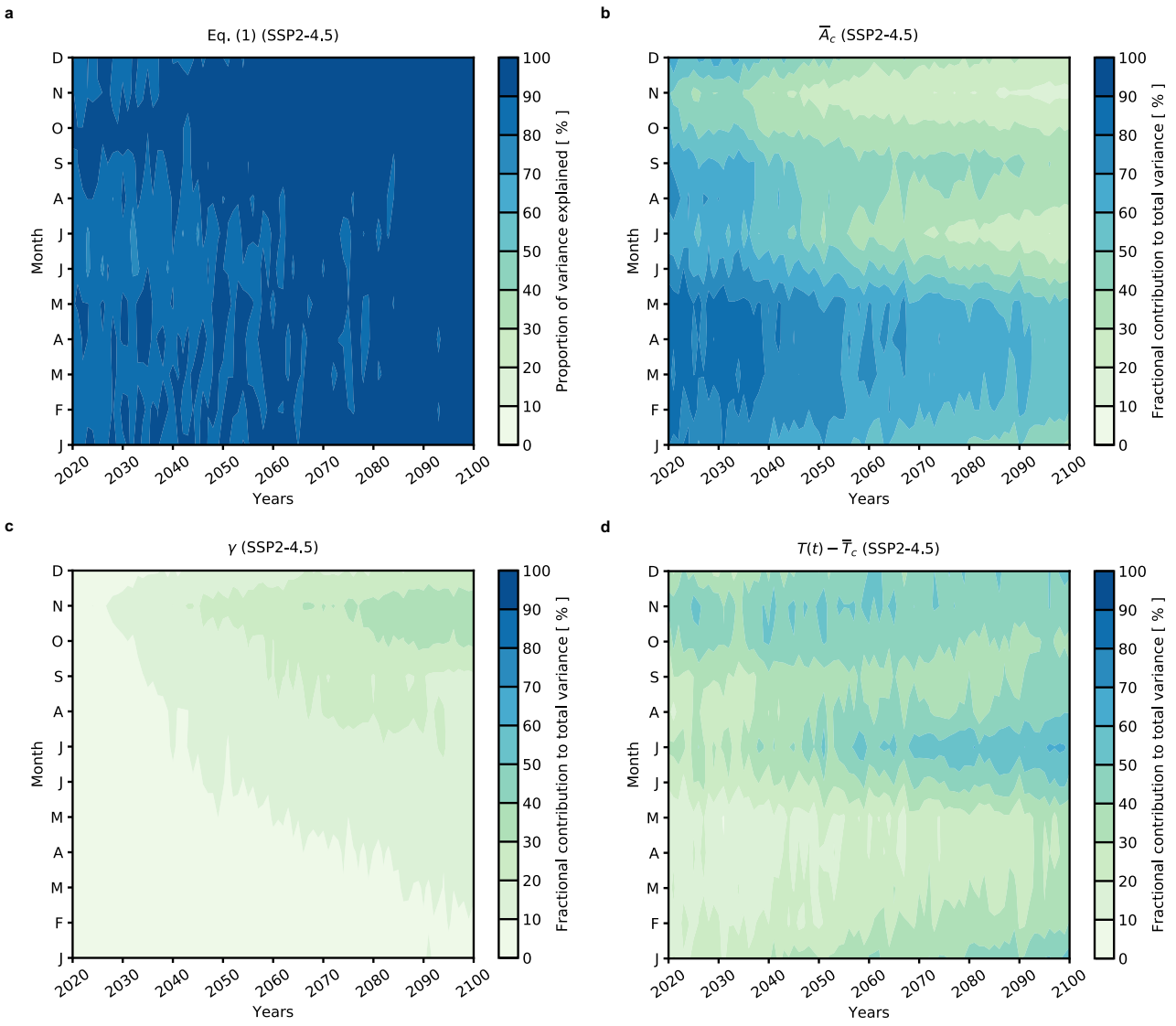

Supplemental Figure 3: **Partitioning intermodel variance in projections of Arctic sea-ice area in SSP2-4.5.** (a) The proportion of the inter-model variance (r^2, where r is the Pearson correlation coefficient) in monthly Arctic sea-ice area from CMIP6 models that is accounted for by Eq. (1) as a function of month and year. Fractional contribution of (b) $\overline{A}_c$, (c) γ, and (d) $T(t) - \overline{T}_c$ to total variance as a function of month and year.

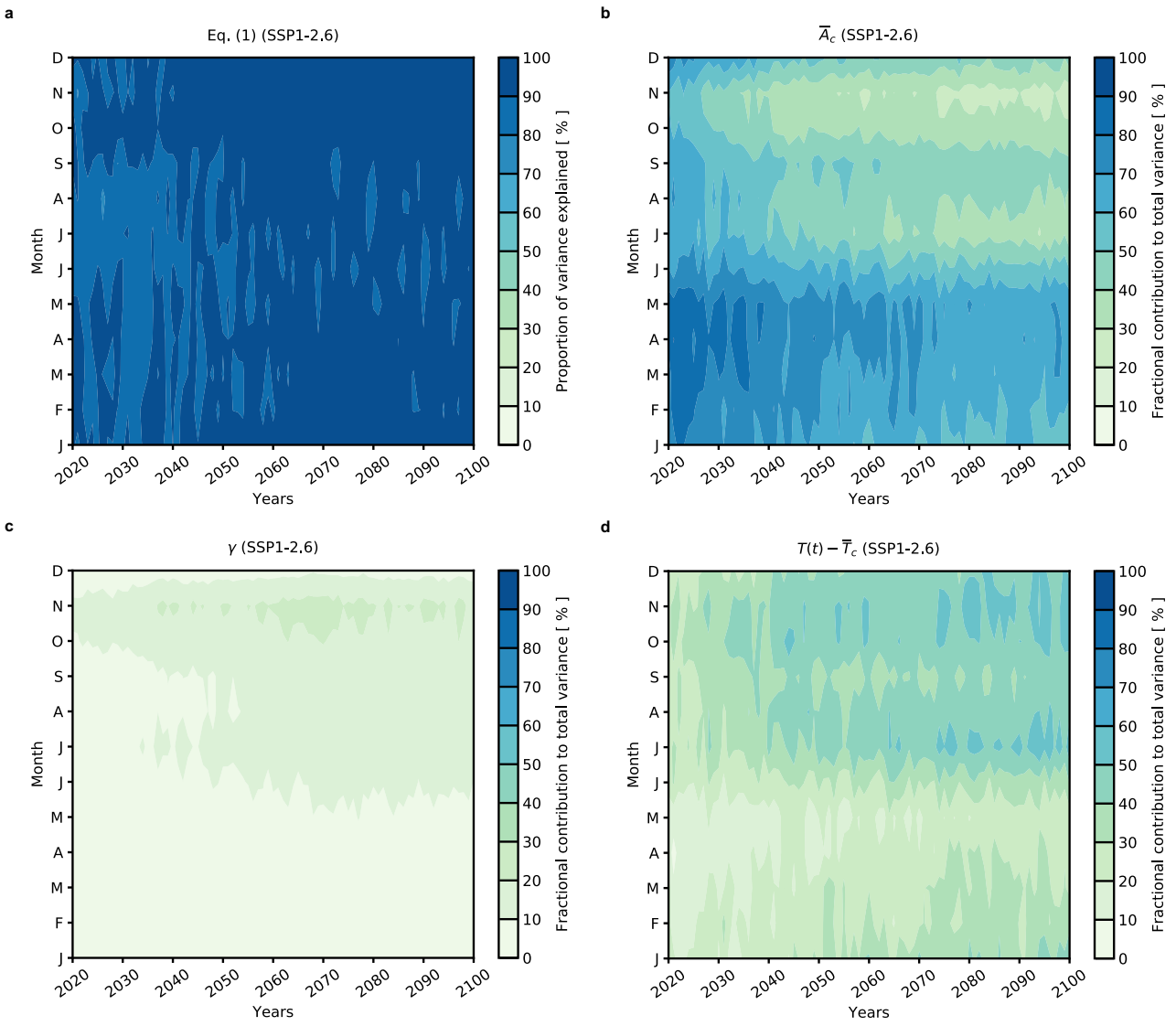

Supplemental Figure 4: **Partitioning intermodel variance in projections of Arctic sea-ice area in SSP1-2.6.** (a) The proportion of the inter-model variance (r^2, where r is the Pearson correlation coefficient) in monthly Arctic sea-ice area from CMIP6 models that is accounted for by Eq. (1) as a function of month and year. Fractional contribution of (b) $\overline{A}_c$, (c) γ, and (d) $T(t) - \overline{T}_c$ to total variance as a function of month and year.

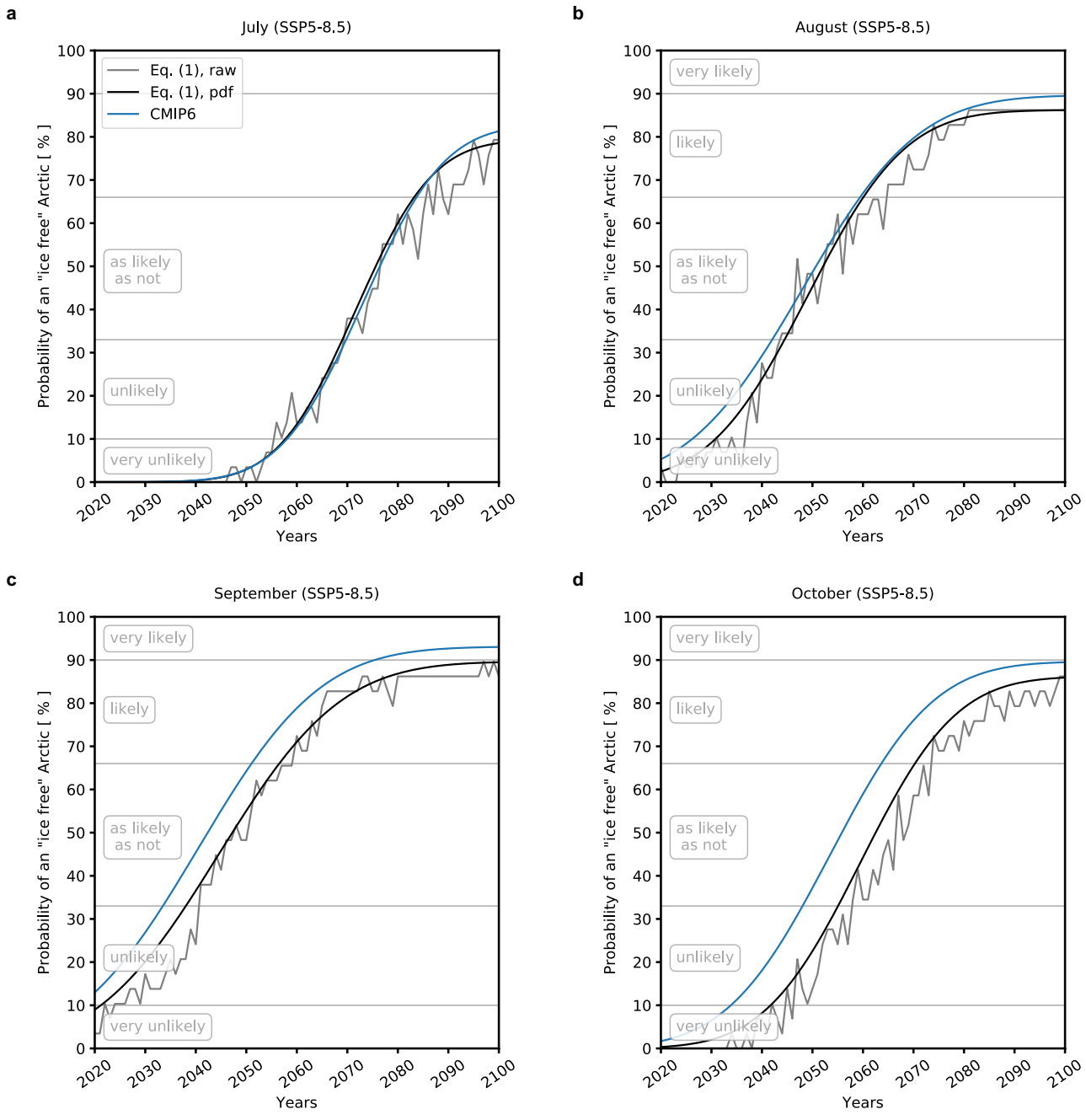

Supplemental Figure 5: **Comparison of GCM and Eq. (1) probabilities.** Cumulative probability density function showing the year when the Arctic will experience ice free conditions in (a) July, (b) August, (c) September, and (d) October. The black line represents Eq. (1), which is identical to Fig. 4, and the blue line is the unconstrained CMIP6 output. The grey line shows the cumulative GCM frequencies.